

GT2011-45098

## FLOW VISUALIZATION AND CONJUGATE HEAT TRANSFER STUDY FROM SHOWER HEAD IMPINGING JETS

Rajesh Kumar Panda

B.V.S.S.S. Prasad\*

Thermal Turbomachines Laboratory  
Department of Mechanical Engineering  
Indian Institute of Technology Madras, Chennai, India

### ABSTRACT

Computational and experimental investigations on a flat circular disk are reported with a constant heat flux imposed on its bottom surface and a shower head of air jets impinging on the top surface. The shower head consists of a central jet surrounded by four neighboring perimeter jets. Lamp black flow visualization technique and computations using shear stress transport (SST)  $\kappa\text{-}\omega$  turbulence model are employed to describe the complex interaction of the wall jets and the associated flow structure. Thermochromic liquid crystal measurement technique is used for surface temperature measurement. The formations of saddle point, nodal point of attachment, nodal point of separation, flow separation line and the up-wash flow are identified. It is observed that the flow topology is practically independent of Reynolds number within the investigated range but is significantly altered with the spacing between the jet orifice and the target surface. A strong correlation between the Nusselt number and the pressure distribution is noticed. Local variation of heat transfer rate with varying plate spacing to jet diameter ratio is significant but its effect on the area weighted average heat transfer rate is small. When compared with a single jet of equal mass flow rate and Reynolds number, the shower head jets provide higher heat transfer rate but require more power for pumping.

**Keywords:** Jet impingement, Shower head, conjugate heat transfer, TLC measurement, CFD, Flow visualization.

### 1. INTRODUCTION

Impinging jets are used for intense localized cooling of hot surfaces. Conventionally, a target plate of size  $L$  is cooled with a single jet of diameter  $D$  if the aspect ratio  $L/D$  is less than 10. On the other hand, for a larger aspect ratio, arrays of jets arranged in either staggered or in-line fashion are used. The important difference between the flow characteristics of various arrangements of impinging jets arises due to the difference in flow resistance offered by neighboring jets. Huber and Viskanta [1] pointed out this fact as early as 1994, in a study pertaining to array of in-line/staggered jets. Similar observations were also

made later by other experimental investigators e.g. Garimella and Schroeder [2]. Exhaustive survey of literature on multiple jet impingements are made by Martin [3] and recently by Weigand and Spring [4]. It appears that there are only a couple of investigations reported on the shower head arrangement. Aldabbagh and Sezai [5] studied laminar jets emanating from square holes with isothermal boundary condition imposed on the impingement plate. Panda et al. [6] showed that, when five jets were arranged in a shower head fashion the target surface exhibits a more uniform temperature distribution, compared to the single jet case.

Sagot et al. [7] compared the computational results obtained by various authors who used different RANS models, and recommended the usage of  $\kappa\text{-}\omega$  SST turbulence model. Similar recommendation was also made by Ramakumar and Prasad [8] for a concave curved surface. Sagot et al [7] noted that the maximum difference in Nusselt number values calculated with constant heat flux and constant temperature boundary conditions was 12%. Katti and Prabhu [9] reported local Nusselt number variation by imposing constant heat flux condition on a very thin foil plate, where the heat conduction could be neglected. Likewise, a large number of jet impingement investigations on single jet [10-12] and on multiple jets [13-15] were reported, without considering the heat conduction within the plate. However, in practice, the thermal boundary conditions cannot be simply specified as constant temperature or constant heat flux, because the impingement heat transfer takes place together with heat conduction in the plate. Thus, this is strictly a conjugate problem. It is evident from the references such as [16] and [17] that thermal conductivity and thickness ratios dictate whether the conjugate study is important or not. In order to address this aspect, Siba et al. [18] constructed an experimental model with 12.7 mm thick stainless-steel plate and used inverse heat conduction technique to calculate both surface temperature and heat flux by feeding measured temperature at 0.76 mm below the top surface. With the objective of studying the conjugate heat transfer, Yang and Tsai [19] used low Reynolds  $k\text{-}\omega$  turbulence model to predict the heat transfer coefficient for the

\*Professor and author of correspondence; e-mail: prasad@iitm.ac.in

flat plate model of Siba et al. [20]. They predicted top (impingement) surface temperature variation by imposing different uniform heat flux values at the bottom surface. Panda and Prasad [21] showed the importance of conjugate condition for the accurate estimation of surface temperature or heat flux.

All the reported investigations in the foregoing papers pertain only to the single jet or in-line/staggered arrays. It is evident from the above literature that the topological information of flow and temperature patterns on an impingement surface with five jet turbulent shower head configuration have not been reported to explain the thermo fluid characteristics. The broad objectives of the paper are therefore to report for the shower head geometry, (i) topological description of the flow structure and temperature patterns through both experimental (oil-lampblack flow visualization and TLC measurement) and computational means, (ii) the effect of varying  $H/d$  and Reynolds number on heat transfer and pressure distribution, and (iii) a typical case of comparison between pressure distribution and heat transfer rates from single jet and shower head.

## NOMENCLATURE

$d$	Jet orifice diameter in case of shower head jet, m.
$D$	Jet orifice diameter in case of single jet, m.
$H$	Height of the orifice from plate, m.
$h$	Heat transfer coefficient, $q''/A(T_w-T_{oe})$ , $W/m^2.K$
$k$	Thermal conductivity ( $W/m-K$ )
$l$	Pitch circle diameter of the perimeter jet, m.
$L$	Characteristic length of the impingement plate
$Nu$	Nusselt Number, $(h \times d)/k$
$P$	Pressure, Pa
$q''$	Wall heat flux, $W/m^2$
$Re$	Reynolds number, $\rho v d / \mu$
$r$	Radial co-ordinates
$R$	Radius of the plate, m
$t$	Thickness of the plate, m
$T$	Temperature, K
$V_{oe}$	Orifice exit jet velocity, m/s
$V_z$	Vertical velocity, m/s
$V_r$	Radial velocity, m/s
$V_\theta$	Angular velocity, m/s
$u, v, w$	Velocity component in x, y and z direction respectively, m/s
$y^+$	Dimensionless wall distance

### Greek Symbol

$\kappa$	Turbulent kinetic energy, $m^2/s^2$
$\nu$	Kinematic viscosity, $m^2/s$
$\omega$	Specific dissipation rate, $1/sec$

### Subscript

amb	Ambient
f	Fluid
max	Maximum
min	Minimum
oe	Orifice exit
s	Solid
w	Wall

## Abbreviations

RGB	Red Green Blue
SIMPLE	Semi-Implicit Method for Pressure-Linked Equations
SST	Shear Stress Transport
TLC	Thermochromic Liquid Crystal

## 2 EXPERIMENTAL DETAIL

The schematic layout of the experimental set up is shown in Fig. 1. Air is supplied by a reciprocating air compressor (1) through a calibrated rotameter (2). Air filter (3) and pressure regulator are installed upstream of the rotameter to filter the air and to maintain the downstream pressure. Air filter removes the moisture and dust particles from the incoming air. Flow regulating and bypass valves (4) are placed in supply line to control the flow rate. Air enters by a flexible pipe (5) through diverging section (6) to reduce the velocity of air into the plenum chamber (7). The plenum chamber's size is large enough to stabilize the flow and provide uniform velocity at jet exit. Air from plenum chamber enters into the impingement chamber (8) which is made of 160 mm diameter, 250 mm height and 4mm thick mild steel cylinder. Air ejects as jet through five, 10mm diameter orifice and impinges on the target surface (9). There is centre hole and rest four holes are placed  $90^\circ$  apart from each other, as shown in Fig. 2. The impingement plate (160 mm diameter and 20 mm thickness) is heated (10) from the bottom surface and circumferentially insulated (11). The plate is made up of mild steel (12). Impingement plate and heating element are placed over a stand (13), whose height can be varied by a lead screw mechanism to obtain the required  $H/d$ . The power input to the heating coil is controlled by a variable auto-transformer (14) and measured by precision voltmeter and ammeters (15). The impingement plate is instrumented with pre-calibrated T-type thermocouples (16). Agilent 34970A (HP make) (17) and personal computer (18) with required software are used for data acquisition.

In order to study the topology of flow pattern, flow visualization experiments are carried out with oil-lampblack technique. The oil and lampblack powder are mixed in proper proportion and painted on the surface of the target plate. The lampblack coated target surface is kept beneath the impingement chamber, as shown in Fig. 1. The air jets, after impinging on the target surface, leave traces of the flow pathlines on the plate. These pictures are captured by a camcorder.

Hallcrest make thermal liquid crystal (TLC) sheet R45C10W, is pasted on the top surface of the target plate. The temperature distribution of the target plate surface can be gauged through the colored (RGB) image of the liquid crystal. The range of measurable temperature of the TLC is chosen to be between 315K and 331K with the middle temperature of 323K corresponding to green color. The uncertainty in this measurement of temperature is  $\pm 0.1^\circ K$ . Assuming  $\pm 5\%$  uncertainty in heat flux value on the target surface, the uncertainty in heat transfer coefficient is less than  $\pm 6\%$ .

The digital camcorder is securely placed over the test section to obtain the RGB images from the TLC. Care has been

taken not to alter lighting and viewing angles throughout the calibration as well as actual test. A small region of interest on the plate is selected for constructing the calibration curve. The calibration has been carried out by considering the temperature at a point close to this region and recorded using a thermocouple located 0.5mm below the surface. Although the minimum size of the region of interest is a single pixel, to account for noise five pixels are considered around the chosen point while estimating the value of hue [20]. MATLAB r2009b image processing tool box used to convert the RGB values of the images to hue. The images are stored as two-dimensional arrays, in which each element of the matrix corresponds to a single pixel in the displayed image. The images taken during the experiment require a three-dimensional array, where the first plane in the third dimension represents the red pixel intensities, the second plane represents the green pixel intensities, and the third represents the blue. A calibration curve of temperature versus hue is constructed as shown in Fig. 3. Notice that fifth order polynomial is used to fit the data relating hue and temperature. This curve is used to estimate the value of surface temperature at each location during actual experiment.

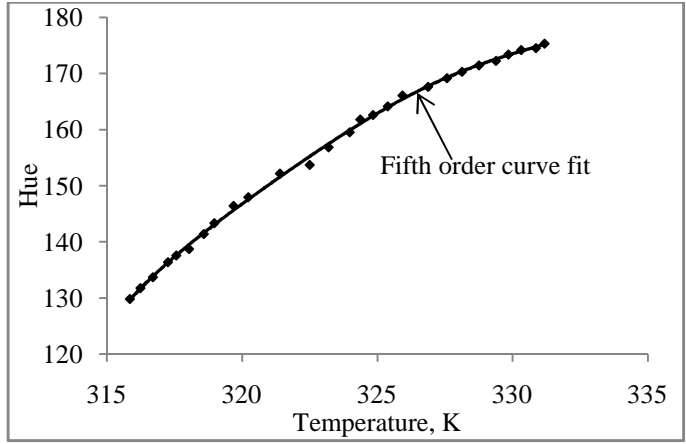


Fig. 3 TLC calibration curve between temperature and hue

### 3 COMPUTATIONAL METHODOLOGY

Figure 4 shows the geometric model that mimics the physical model used in the experiments described in the previous section. The bottom part of the impingement chamber consists of a semi-confined circular plate with five circular orifices of 10 mm diameter, representing the shower head. The target plate on which the jets impinge is a 160 mm diameter 20 mm thick mild steel plate. The jets eject from the circular orifices to impinge on the solid plate. Distance between the impingement plate and the top wall is so varied as to obtain the H/d ratio from 1 to 4.

The computational model can be divided into the fluid zone and the solid zone. The computational mesh suitable for finite volume method is generated by automatic grid generating tool GAMBIT 2.3.16. Non-uniform grids with clustered nodes are generated in the regions where steep gradient of temperature is expected. Hexahedral structure is used for meshing. Optimum grid size is selected after the grid independence study. The grid sizes finally chosen are: 1.8million for H/d= 1; 2.3 million for H/d= 2; and 2.7 million for H/d = 4. The values of maximum  $y^+$  used in the present computations are around 1. Figure 5 shows the mesh used for H/d = 4.

For the purpose of computation, a specified velocity inlet condition is imposed at the entry to the orifices. A free stream turbulence intensity of 6% is chosen at the exit of orifice. The jets, after hitting the plate, exit into the atmosphere in transverse direction, all around the plate periphery, where constant (ambient) pressure outlet condition is imposed. A constant heat flux value is specified at the bottom surface of the target plate and the periphery is circumferentially insulated. All the input values are those used in experiments.

The three dimensional conjugate heat transfer problem is formulated with the following assumptions: (i) the fluid is incompressible, (ii) the fluid properties are constant (iii) radiation and natural convection are neglected, (iv) viscous dissipation is absent and (v) the flow is steady. The governing equations used for simulation are the Reynolds averaged continuity, momentum and the energy equations along with the equations for modeling the turbulence quantities.

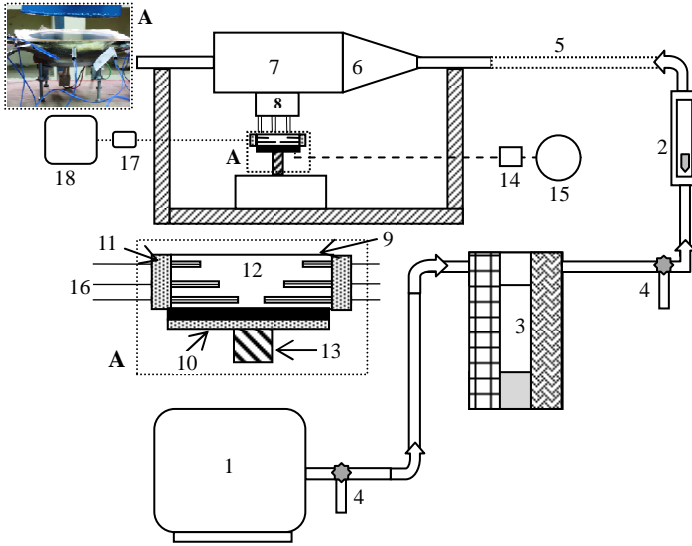


Fig. 1 Schematic diagram of experimental set-up

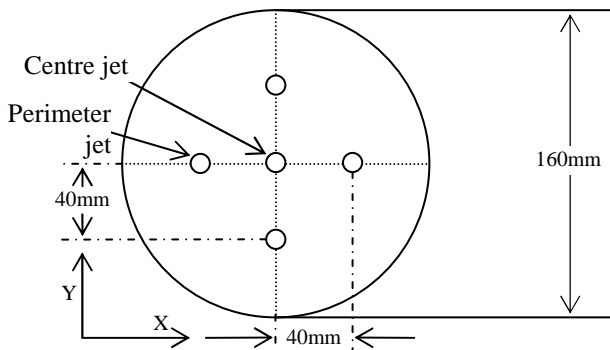


Fig. 2 Arrangement of impingement jet

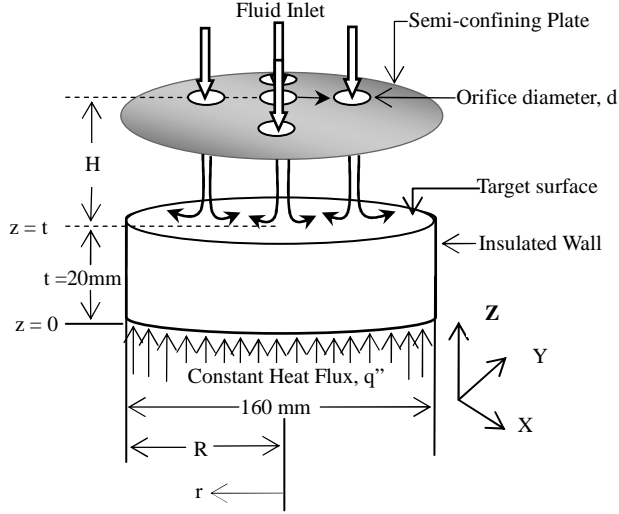


Fig. 4 Schematic of the geometry and boundary conditions

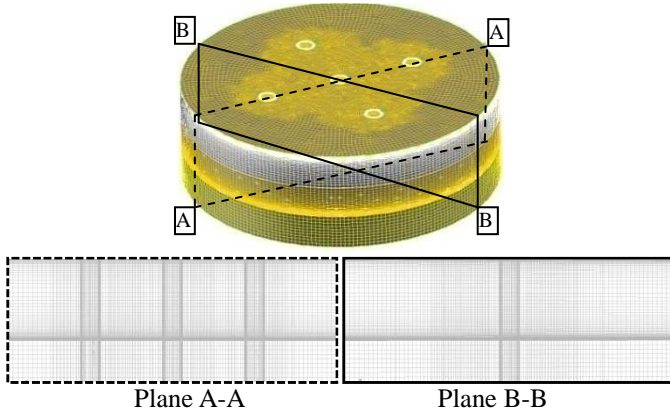


Fig. 5 Mesh used for  $H/d = 4$

Boundary conditions used for the present study are,

i) No slip boundary condition

$$V_w = 0, \text{ at } z = t \text{ and semi-confining plate}$$

ii) Flow inlet condition,

$$V_r, V_\theta = 0, V_z = V_{oe} \text{ and } T_{oc} = 300K$$

iii) Entrainment condition,

$$P = P_{amb}, \text{ at } r = R, 0 < z < H$$

iv) Conjugate boundary condition,

$$T_s = T_f$$

$$k_s \frac{\partial T_s}{\partial Z} = k_f \frac{\partial T_f}{\partial Z} \quad \text{at } z = t$$

v) Constant heat flux condition,

$$-k_s \frac{\partial T_s}{\partial z} = q'', \text{ at } z = 0, 0 < r < R$$

vi) Adiabatic condition,

$$\frac{\partial T_s}{\partial r} = 0, \text{ at } r = R, 0 \leq z \leq t$$

A finite volume based solver Fluent 6.3 is used for solving the governing continuity, momentum, energy and turbulence model equations. SIMPLE algorithm is used for pressure

velocity coupling. The solution is considered to be converged when the maximum residual value is in the order of  $10^{-4}$  for continuity, momentum and turbulence equations and  $10^{-6}$  for energy equation. The  $\kappa\text{-}\omega$  SST model is adopted for simulation. Further, area weighted average of temperature of the impingement surface is continuously monitored, so that the variation will be within 0.1% for 1000 consecutive iterations. Simulation continued till solid plate reaches steady state.

The parameters investigated in the present study include (i) effect of  $H/d$ , varied as 1, 2 and 4, and (ii) effect of jet exit Reynolds number, varied as 7115, 8299, 9500 and 10672. Diameter of the shower head jet orifice is kept constant as 10 mm.

## 4 RESULTS AND DISCUSSION

### 4.1. Topology of flow pattern

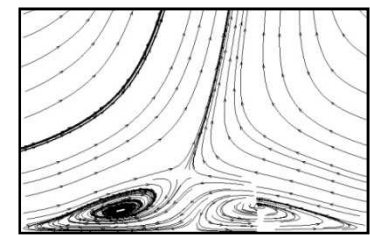
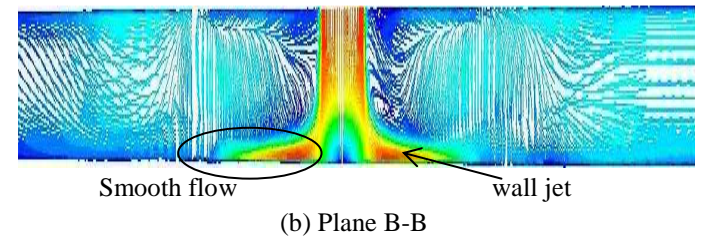
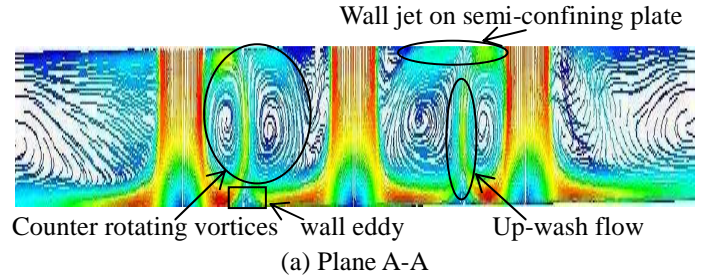
As each fluid jet ejects out of the orifice with uniform velocity profile a continuous reduction in velocity takes place from its centre line to the outer boundary. It is known that with increasing distance from the exit, and increasing momentum exchange between the jet and the ambient the free boundary of the jet broadens while the potential core contracts. On the impingement surface the wall jets are formed and spread radially. The wall jet emanating from each impinging jet forms a collision front due to its interaction with the neighbors. Consequently an up-wash flow takes place. Thus overall flow structure consist of (i) potential core, (ii) shear layer, (iii) wall jets, (iii) up-wash flow etc. This overall flow structure depends on the configuration of jets as discussed in ref. [4]. However the topology of the flow pattern is represented by oil streaklines or skin friction contours. The topology for three  $H/d$  values is discussed in the following section.

#### 4.1.1. $H/d = 1$

The skin friction lines and the path lines on the impingement surface for the case of  $H/d = 1$  are shown in Fig. 6. Referring to Fig. 6 (a), when the shear stress value is too small, then the oil will not be able to move the lamp black and hence those areas look darker. Figure 6 (b) reveals that the computationally obtained topology of flow pattern on the impingement surface agrees well with the experiment. A zoomed view of the west centered part of Fig 6 (b) shows nodal point of attachments, saddle points, separation lines and attachment lines. For the present configuration, there are five nodal points of attachment (NA1 to NA5) each corresponding to the location of impingement (or stagnation point) on the surface, where all skin friction lines are directed outward. As the shear stress value is low at NA, a dark patch is noticed near NA. Due to the interaction of two wall jets two saddle points are formed. The saddle point (denoted by SP in Fig. 6 (b)) is a singular point through which only two particular lines (CC and DD) can pass. The directions on either side of the singular point are inward on one particular line (CC) and outward on the other particular line (DD). As the two saddle points SP1 and SP2 cannot be joined together [21], four attachment lines AL1 to AL4 from which the skin friction lines tend to diverge, are

formed. The diverged flow from the line of attachment and nodal point of attachment prevents each other to pass through the saddle point and finally ends up forming another line termed as the line of separation denoted by SL.

The line of separation, which has a saddle point on it, makes a necessary condition for flow separation [21]. The wall jets, thus separated from each other in the impingement plane at the separation line, are shown in Fig. 7 (a) along plane A-A (please refer Fig. 5). The upwash flow impinges on the top wall to form low velocity wall jet. The top wall jet is then entrained into the main jet stream leading to the formation of two counter rotating vortices, shown in Fig. 7 (a). The upwash flow forms from the saddle point between the centre jet and the perimeter jet. Whereas in case of plane B-B no such upwash flow observed and the centre jet spreads smoothly radially outward, shown in Fig. 7 (b). Another pair of ring shaped eddies called as wall eddy are formed between the counter rotating toroidal vortices and the target surface. Wall eddy forms from the attachment line which merges towards the saddle point in opposite direction. Due to this, the wall eddies rotate in opposite directions as shown in Fig. 7 (c).



(c) Wall eddies near upwash flow (Zoomed view of Fig. 7 (a))

Fig. 7 Three dimensional separation, for  $H/d = 1$  and  $Re = 9500$

**4. 1. 2.  $H/d = 2$**

The formation of nodal point of separation (NS) and absence of wall jet on top wall are the striking features for topology of flow pattern for  $H/d = 2$ , Fig. 8.

At the nodal point of separation NS, all the skin friction lines are directed inward (as opposed to NA where the lines are outward) towards the node. This makes a necessary condition for flow separation [21]. For the case of  $H/d = 2$ , nodal points of separations are observed (Fig. 8 (b)) along plane B-B. As shown in Fig. 8 (b), there are four saddle points and four nodal points of separation forming a quadrilateral shaped skin friction contour around the centre jet. Due to reflection of camera in some cases separation lines between the perimeter jets are not clearly observed. At the nodal point of separation the flow separates and lifts up, as shown in Fig. 9 (a). As a result, there is a formation of vortex (in plane B-B) between the nodal point of separation and centre jet for  $H/d = 2$ . It may be recalled that for  $H/d = 1$  no nodal point of separations are noticed (Fig. 6 (b)) and hence the flow has smoothly spread plane B-B, as shown in Fig. 9 (b).

When  $H/d = 2$  the up-wash flow cannot reach the top plate. As a result the upper wall jets do not form, as noticed in Fig. 9 (b).

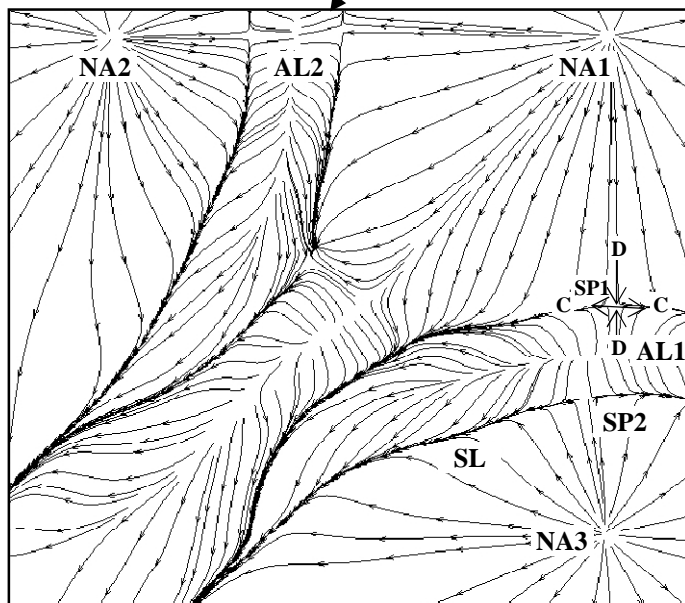
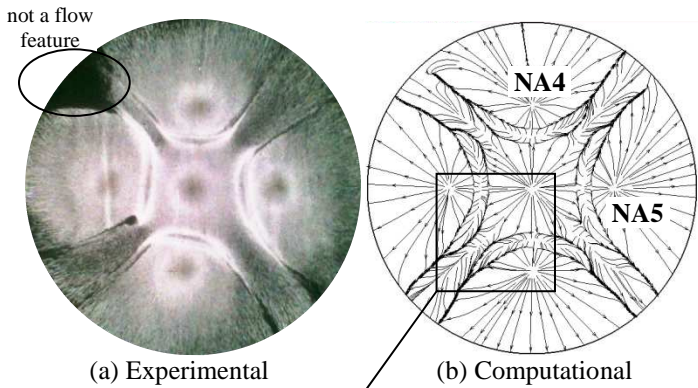


Fig. 6 Flow topology, for  $H/d = 1$  and  $Re = 9500$

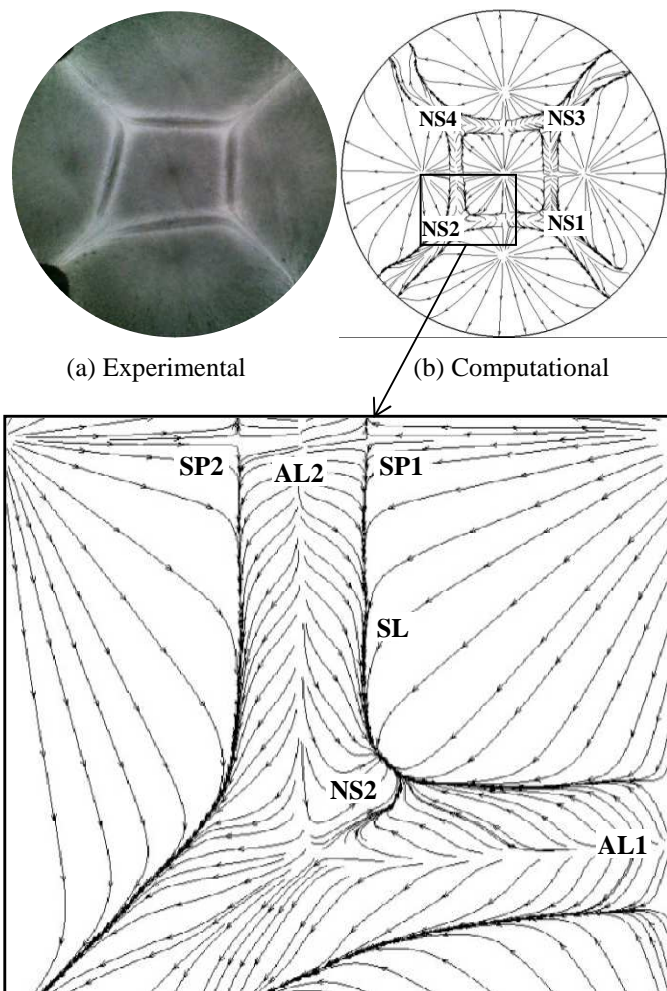
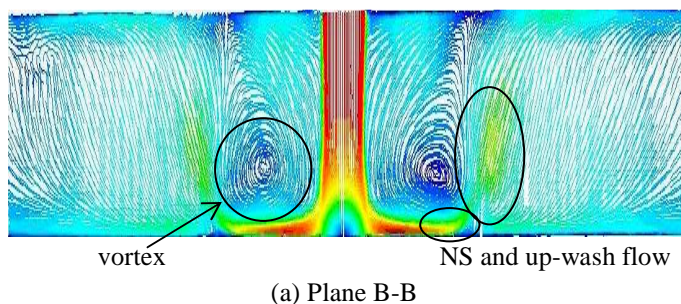
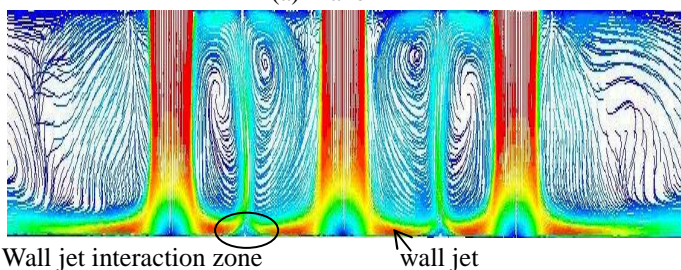


Fig. 8 Flow topology, for  $H/d = 2$  and  $Re = 9500$



(a) Plane B-B



(b) Plane A-A

Fig. 9 Three dimensional separation, for  $H/d = 2$  and  $Re = 9500$

#### 4. 1. 3. $H/d = 4$

As  $H/d$  increases, the momentum of the jet striking the target surface decreases. As a consequence, the size of the quadrilateral shaped skin friction contour also decreases for a given Reynolds number. Otherwise, the topology of flow pattern resembles the one for  $H/d = 2$ .

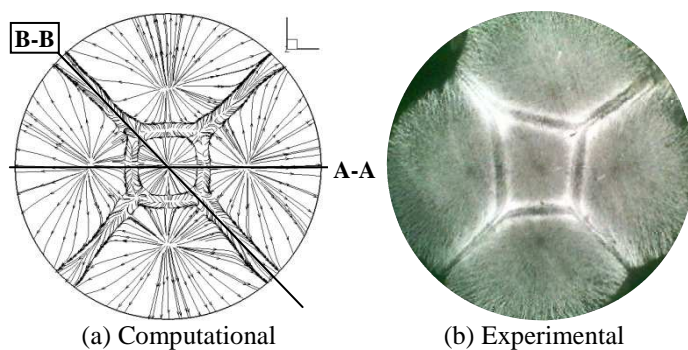


Fig. 10 Flow topology, for  $H/d = 4$  and  $Re = 9500$

It is observed that the skin friction lines are almost independent of Reynolds number, in the range of 7115 to 10674, refer Fig.11.

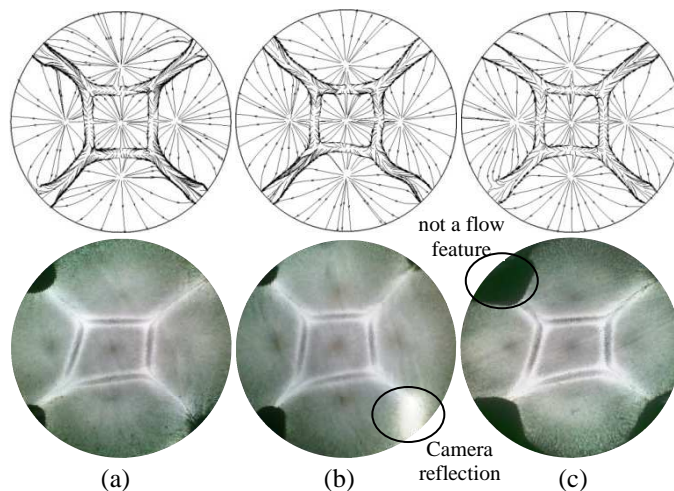


Fig. 11 The skin friction lines on the impingement surface, for (a)  $Re = 10674$ , (b)  $Re = 8299$  and (c)  $Re = 7115$  at  $H/d = 2$

#### 4.2 Topology of temperature pattern

Figures 12 and 13 show the steady state surface temperature distribution of the 20mm thick impingement plate for  $H/d = 4$ ,  $q'' = 3000 \text{ W/m}^2$  and  $Re = 9500$ , obtained from TLC measurement and computations respectively. Dotted zone in Fig. 13 corresponds to the area where TLC measurement is taken. The green colored zones, which show lower temperature, correspond to the areas of jet impingement and wall jet interaction. The blue colored zones correspond to the areas between the perimeter jets. Similar temperature variation is observed from the computation (Fig. 13). As constant heat flux

is supplied to the bottom surface and top surface is exposed to the shower head jet, the heat flux distribution on the top surface cannot be estimated from the experiment. The overall temperature variation across the surface in both the cases is around 1.5K and the temperature distribution is observed on the impingement surface both from the experiment and computation agreed with each other within  $\pm 3\%$ . Figure 14 shows the comparison between the computational and experimental data, across line x-x. The validity of the computational model for the conjugate heat transfer problem is ascertained.

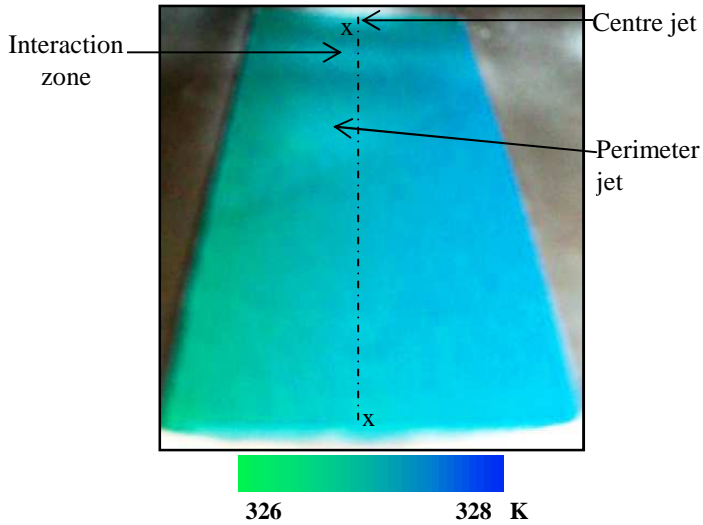


Fig. 12 Surface temperature distribution from TLC technique; for  $H/d = 4$ ,  $q'' = 3000 \text{ W/m}^2$  and  $Re = 9500$

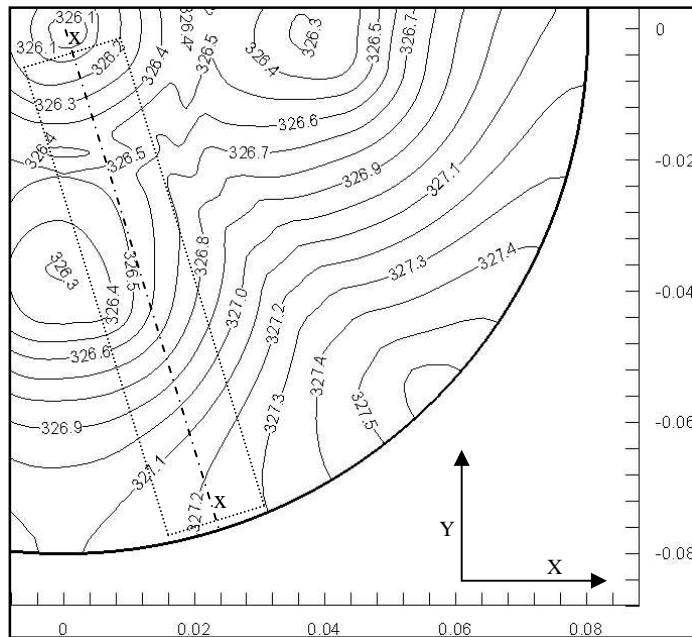


Fig. 13 Surface temperature distribution from computation; for  $H/d = 4$ ,  $q'' = 3000 \text{ W/m}^2$  and  $Re = 9500$

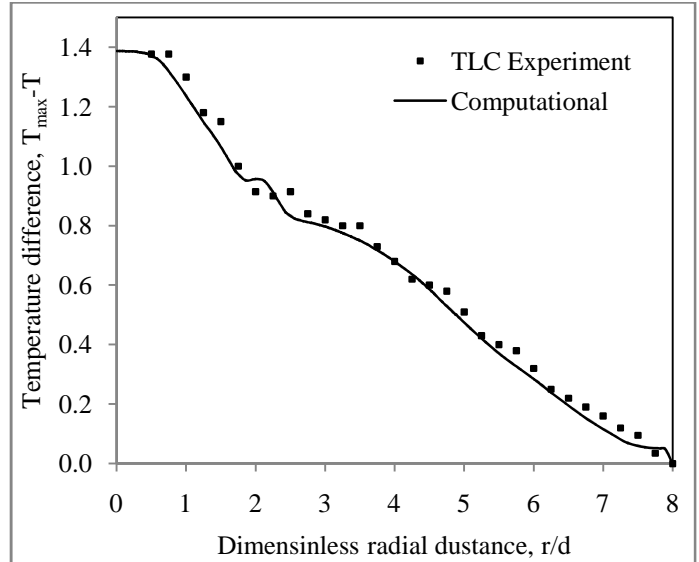
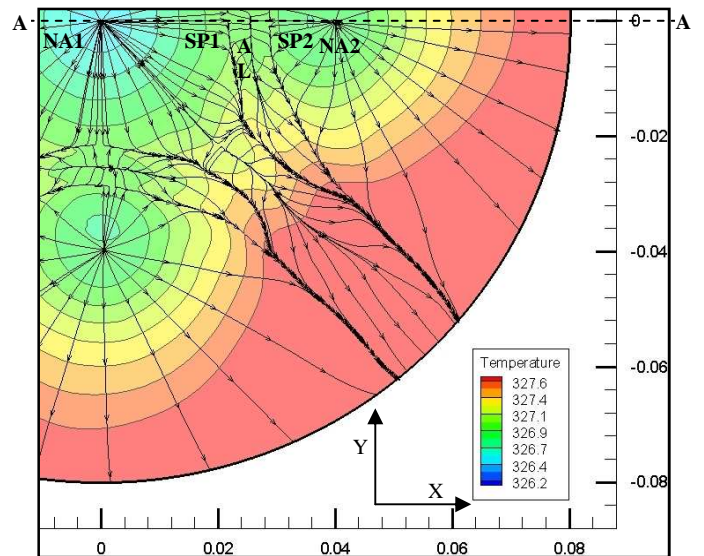
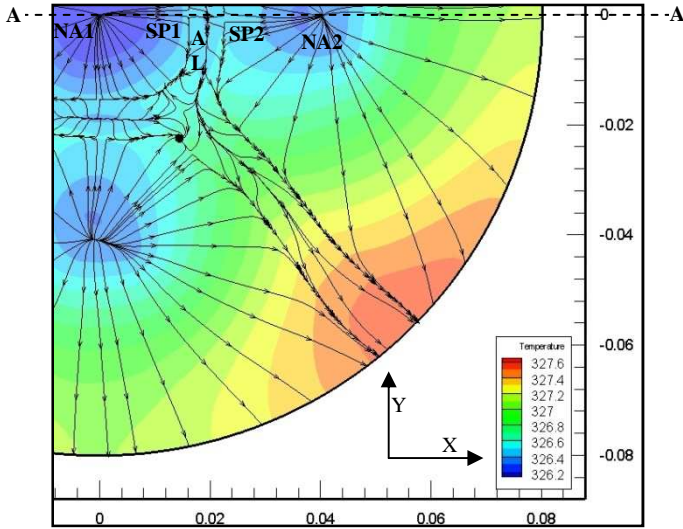


Fig. 14 Temperature distribution across line x-x; for  $H/d = 4$ ,  $q'' = 3000 \text{ W/m}^2$  and  $Re = 9500$

Figure 15 (a, b) shows the computationally obtained temperature contours with the skin friction lines superimposed. Along A-A minimum temperature is maintained at stagnation point of centre jet (NA1). The temperature increases upto the saddle point (SP1) and thereafter decreases upto the attachment line (AL). On the other hand the temperature is low at the stagnation point of the perimeter jet (NA2) and increases upto SP2 then decreases upto AL. The wall eddies are responsible for enhancement of local heat transfer and decrease of temperature along AL. The temperature variation across the plate surface is around 2K. But the heat flux variation on the target surface has a wide variation, shown in Fig. 16 (a, b). The heat flux values are larger where cooling rates are higher, e.g. at the nodal point of attachments and the interaction zones. The variations in heat transfer are graphically shown in Fig. 17.

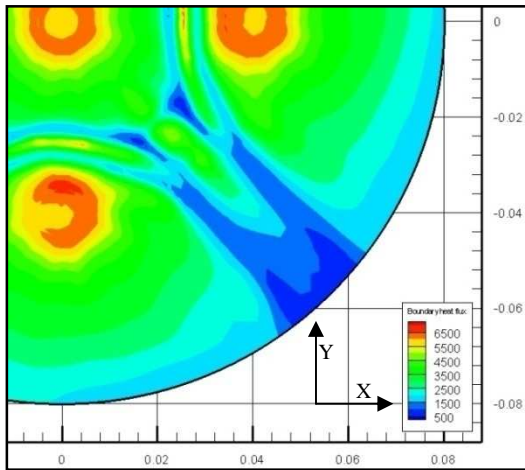


(a)  $H/d = 1$

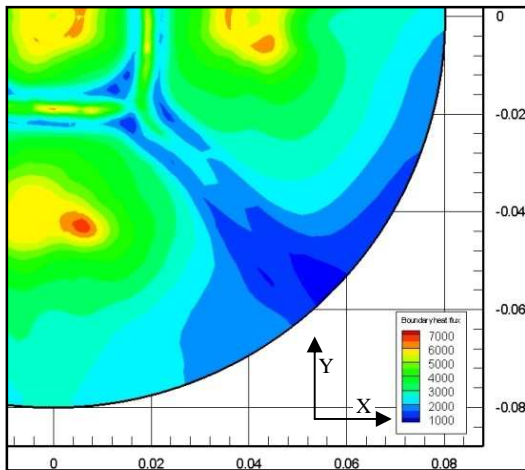


(b)  $H/d = 4$

Fig. 15 Temperature contour with skin friction lines obtained from CFD; for varying  $H/d$ ,  $q'' = 3000 \text{ W/m}^2$  and  $Re = 9500$



(a)  $H/d = 1$



(a)  $H/d = 4$

Fig. 16 Heat flux contour obtained from CFD; for varying  $H/d$ ,  $q'' = 3000 \text{ W/m}^2$  and  $Re = 9500$

### 4.3 Effect of plate spacing to jet diameter ratio ( $H/d$ )

The effect of plate spacing to jet diameter ratio ( $H/d$ ) for  $Re = 9500$  and  $q'' = 3000 \text{ W/m}^2$  in plane A-A is shown in Fig. 17. Although the temperature difference across the plate surface is low heat flux has a wide variation, due to which variation in Nusselt number observed. For higher  $H/d (= 4)$ , the maximum Nusselt number value in the stagnation region is lower compared to lower  $H/d (= 1)$  by about 6 - 7%. The difference among Nusselt numbers at the centre jet is less compared to the perimeter jet, because the perimeter jets are more affected by low temperature quiescent ambient air. The secondary peaks are observed at AL (the interaction region of the wall jets of centre and perimeter jet). The upwash fountain for lower  $H/d$  is more prominent hence larger secondary peaks are observed for lower  $H/d$ . The radial shift in the position of the secondary peaks is due to the decrease in size of the quadrilateral around the centre jet.

Another interesting observation regarding these Nusselt number variations can be made by comparing them with the computed pressure distribution, shown in Fig. 18. Mohanty and Prasad [22] indicated that the heat transfer value is co-relatable with the pressure gradient. The closeness of the Nusselt number pattern in Fig. 17 with the dimensionless pressure gradient ( $P^* = \text{Static pressure}/\text{Maximum static pressure}$ ) pattern in Fig. 18 indicates this proposition. The shift in the Nusselt number curves follows closely the shifts in dimensionless pressure values. Besides, the average pressure on the target surface is proportional to the pumping power.

Area weighted average heat transfer coefficient for the  $H/d = 4$  is  $97.4 \text{ W/m}^2\text{K}$  and for the  $H/d = 1$  case is  $100.8 \text{ W/m}^2\text{K}$  over the impingement surface area. In other words, although there are significant local variations of Nusselt number, the average value differs only by 3 - 4 % as  $H/d$  varies from 1 to 4.

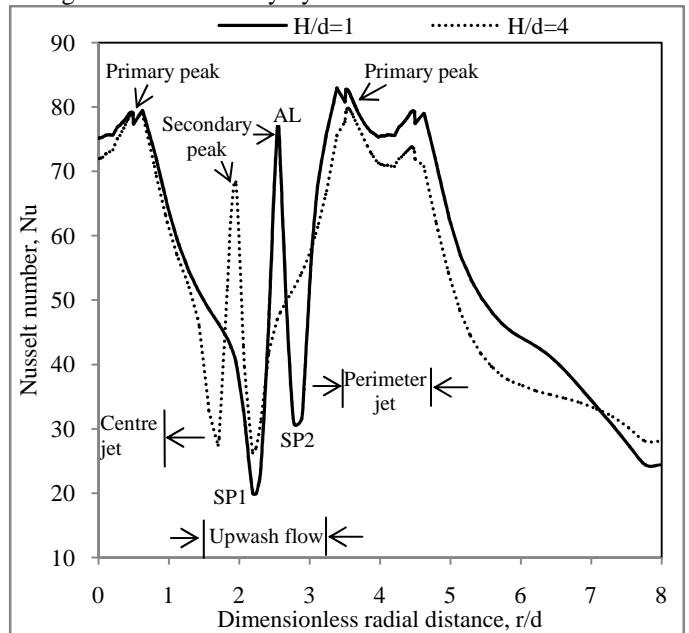


Fig.17 Nusselt number distribution on line A-A obtained from CFD; for varying  $H/d$ ,  $q'' = 3000 \text{ W/m}^2$  and  $Re = 9500$

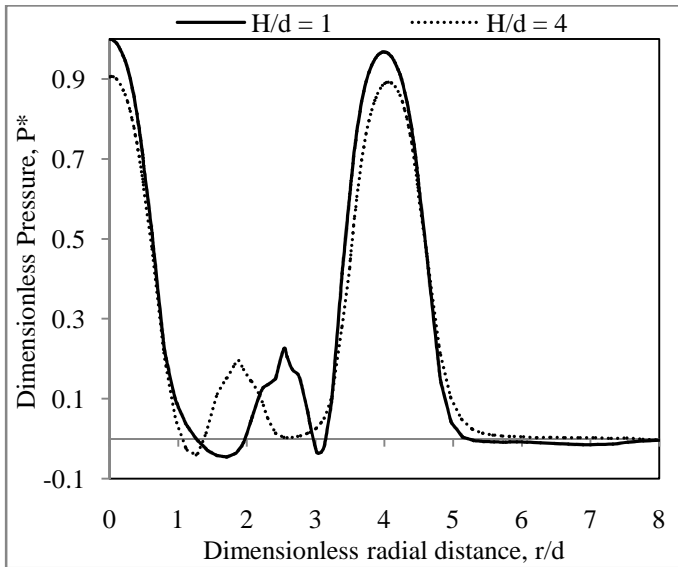


Fig. 18 Computed dimensionless pressure distribution on line A-A; for varying H/d,  $q'' = 3000 \text{ W/m}^2$  and  $Re = 9500$

#### 4.4 Effect of Reynolds number

Figure 19 illustrates the dependence of Nusselt number on Reynolds number for  $H/d = 2$  and  $q'' = 2000 \text{ W/m}^2$  on line A-A. As expected at any location heat transfer rate is higher for high Reynolds number. As discussed earlier with respect to Fig. 11, the flow is independent of Reynolds number in the range of 7115 - 10674. The quantitative behavior of Nusselt number, shown in Fig. 19, clearly indicates that these trends are independent of Reynolds number. Especially the positions of secondary peaks in Nusselt number are found at the same radial location. Area weighted average heat transfer coefficient for  $Re = 7115$  is  $85.3 \text{ W/m}^2\text{K}$  and for  $Re = 10674$  case is  $125.3 \text{ W/m}^2\text{K}$  over the impingement surface area.

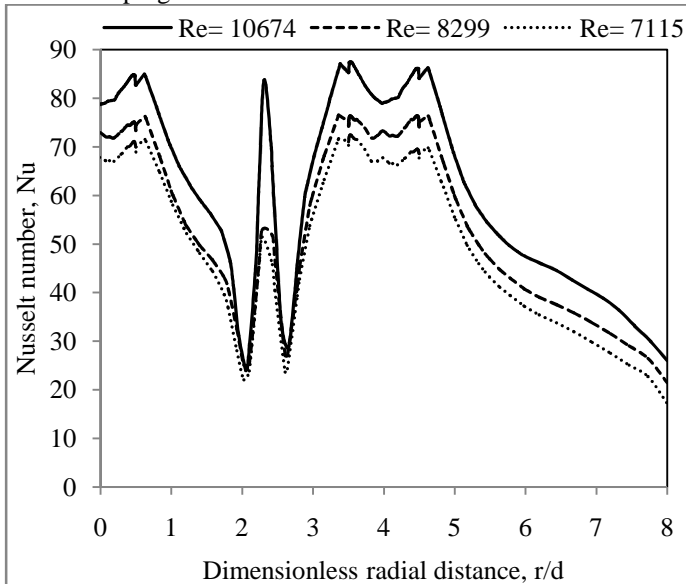


Fig. 19 Nusselt number distribution on plane A-A obtained from CFD; for  $H/d = 2$  and  $q'' = 3000 \text{ W/m}^2 \cdot \text{K}$

#### 4.5 Comparison with single jet

A comparative CFD study is made between the two cases: shower head and single jet configuration to assess the relative merit and demerit. The dimensions for single jet are decided by considering equal mass flow rate for both the cases. Thus the shower head (five) jets of 10mm diameter each are considered equivalent to the single jet of diameter,  $D = 22.36\text{mm}$ . The corresponding height is also changed to maintain the same value of  $H/d$ .

Figure 20 shows the dimensionless temperature ( $T^* = (T - T_{\min}) / (T_{\max} - T_{\min})$ ) variation on the target surface for both jet configurations. On the same figure, the dimensionless pressure variation on the target surface is superimposed. While the temperature curve clearly indicate the shower head is advantageous as the temperature is uniform throughout the surface, the average pressure values shows that the pumping power required for shower head jet is higher.

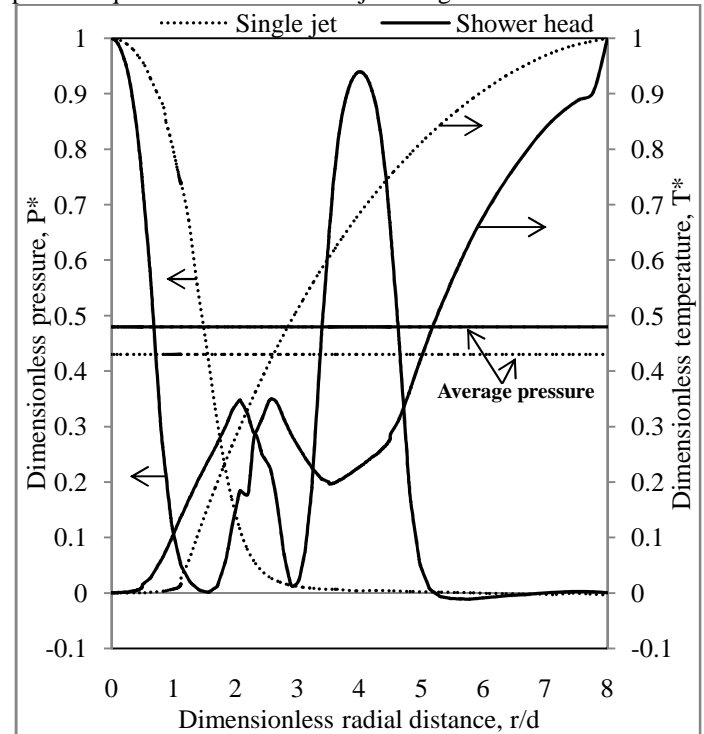


Fig. 20 Dimensionless pressure and temperature distribution on impingement surface obtained from CFD;  $H/d = 2$ ,  $Re = 9500$  and  $q'' = 3000 \text{ W/m}^2 \cdot \text{K}$

#### CONCLUSIONS

Flow topology and conjugate heat transfer of a flat circular disk is investigated with constant heat flux at the bottom surface and with a five-jet showerhead impinging on its top surface. The following conclusions are drawn from the study:

1. The features of the complex flow structure are studied using both by oil-lamp black flow visualization technique and computation. Computationally obtained topology of flow pattern on the impingement surface agrees well with the experiment. The flow structure observed due to the interaction

between the centre jet and perimeter jets are explained by the formation of saddle point, nodal point of attachment and nodal point of separation, the flow separation line, the attachment line, wall eddies and counter rotating vortex. It is observed that the flow topology is independent of the variation of Reynolds number in the range of 7115 – 10674, but is completely altered with variation in H/d.

2. The target surface temperature distribution obtained from TLC is similar to the computational results. This validates the usage of the Shear Stress Transport (SST)  $k-\omega$  turbulence model for the chosen problem. The overall temperature variation across the surface in both the cases is around 1.5K. Lower temperature is observed in the impingement and wall jet interaction zones.

3. The Nusselt number on the surface is found to vary in accordance with the flow structure. Peaks are noticed in the primary and secondary stagnation zones corresponding to the nodal point of attachment and attachment line respectively. Heat transfer is lower at the flow separation point i.e. the saddle point. It is observed that the local heat transfer rate is higher for lower H/d, whereas the area weighted average heat transfer rates are not affected much.

4. Heat transfer rate increases with the increase in Reynolds number. Position of the secondary peak is found to be independent of Reynolds number.

5. The heat transfer variations are clearly co-relatable not only with the flow topology but also with the dimensionless pressure distribution.

6. Shower head jets provide a uniform surface temperature distribution but with higher pumping power compared to single jet, for the same values of mass flow rate, Reynolds number and H/d.

## REFERENCES

- Huber, A.M., and Viskanta, R., 1994, "Comparison of convective heat transfer to perimeter and centre jets in a confined, impinging array of axi-symmetric air jets", *International journal of Heat and Mass Transfer*, Vol. 37, pp. 3025-3030.
- Garimella, S. V. and Schroeder, V.P., 2001, "Local heat transfer distribution in confined multiple air jet impingement", *ASME Journal of Electronic Packaging*, Vol. 123, pp.165-172.
- Martin, H., 1977, "Heat and mass transfer between impinging gas jets and solid surfaces", *Advances in Heat Transfer*, Vol. 13, pg. 1-66.
- Weiband, B. and S. Spring, 2009, "Multiple jet impingement – A review", Int. Symp. on Heat Transfer in Gas Turbine Systems, August 2009, Antalya, Turkey.
- Aldabbagh, L.B.Y., and Sezai, I., 2002, "Numerical simulation of three-dimensional laminar multiple impinging square jets", *International Journal of Heat and Fluid Flow*, Vol. 23, pp. 509–518.
- Panda, R. K., Sreekala P., and Prasad, B.V.S.S.S., 2010, "Computational And Experimental Study Of Conjugate Heat Transfer From A Flat Plate With Shower Head Impinging Jets", *ASME-International Heat Transfer Conference (IHTC-14)*, IHTC14-23188, Washington D.C., USA.
- Sagot, B., Antonini, G., Christgen, A. and F. Buron, 2007, "Jet impingement heat transfer on a flat plate at a constant wall temperature", *International Journal of Thermal Sciences*, Vol. 47, pp.1610-1619.
- Ramakumar B.V.N. and Prasad B.V.S.S.S., "Computational flow and heat transfer of a row of circular jets impinging on a concave surface", *Heat and Mass Transfer*, Volume 44, pp 667-678, 2008.
- Katti, V., and Prabhu, S.V., 2007, "Experimental study and theoretical analysis of local heat transfer distribution between smooth flat surface and impinging air jet from a circular straight pipe nozzle", *International Journal of Heat and Mass Transfer*, Vol. 51, pp. 4480–4495
- Martin, H., 1977, "Heat and mass transfer between impinging gas jets and solid surface", *Advances in Heat Transfer*, Vol. 13, pp. 1–60
- O'Donovan, T. S., and Darina B. M., 2007, "Jet impingement heat transfer – Part 2: A temporal investigation of heat transfer and local fluid velocities", *International Journal of Heat and Mass Transfer*, Vol. 50, pp. 3302-3314.
- Luikov, A. V., 1973, "Conjugate convective heat transfer problems", *International Journal of Heat and Mass Transfer*, Vol.17 pp. 257-265.
- Prasad, B.V.S.S.S., and Sarkar, S. D., 1993, "Conjugate laminar forced convection from a flat plate with imposed pressure gradient", *ASME Journal of Heat Transfer*, Vol. 115, pp. 469-472.
- Siba, E. A., Ganesa-Pillai, M., Harris, K. T. and Haji-Sheikh, A., 2003, "Heat transfer in a high turbulence air jet impinging over a flat circular disk", *ASME Journal of Heat Transfer*, Vol. 125, pp. 257-265.
- Yang, Y-T. and Tsai, S.Y., 2007, "Numerical study of transient conjugate heat transfer of a turbulent impinging jet", *International Journal of Heat and Mass Transfer*, Vol. 50, pp. 799–807.
- Panda, R. K., and Prasad, B.V.S.S.S., 2010, "Computational and experimental study of conjugate heat transfer from a flat plate with an impinging jet." *ASME-TurboExpo2010*, GT2010–22572, June 14-18, 2010, Glasgow, U.K.
- Bansal, G. D., Khandekar, S., and Muralidhar, K., 2009, "Measurement of heat transfer during drop-wise condensation of water on polyethylene", *Nanoscale and Microscale Thermophysical Engineering*, Vol.13, pp: 184 - 201.
- Murray, T., and David J. Peake, 1982, "Topology of three dimensional separated flows", *Annual review of fluid mechanics*, Vol. 14, pp: 39-60.
- Mohanty, A.K, and Prasad, B.V.S.S.S., 1991, "Experimental study of heat transfer from pressure gradient surfaces", *Experimental Thermal and Fluid Science*, Vol. 4, pp: 44-55.